Retinal Tissue Oxygen Tension Imaging in the Rat

Mahnaz Shahidi, Justin Wanek, Norman P. Blair, Deborah M. Little, and Tingting Wu

Purpose. To report an imaging technique for measurement of oxygen tension (PO_2) in retinal tissue and establish its feasibility for measuring retinal PO_2 variations in rat eyes by adjusting the fraction of inspired oxygen (FiO_2).

Methods. A narrow laser line was projected at an angle on the retina, and phosphorescence emission was imaged after intravitreal injection of an oxygen-sensitive molecular probe. A frequency-domain approach was used for phosphorescence lifetime measurements. Retinal PO_2 maps were computed from phosphorescence lifetime images, and oxygen profiles through the retinal depth were derived in rats in conditions of 10%, 21%, and 50% FiO_2.

Results. Retinal PO_2 measurements were repeatable, and variations in outer and inner retina PO_2 at different locations along the image were not significant ($P \geq 0.3$). Maximum outer retinal PO_2 obtained in 10%, 21%, and 50% FiO_2 were significantly different ($P < 0.0001$). Maximum outer retinal PO_2 correlated with systemic arterial PO_2 ($R = 0.70$; $P < 0.0001$). The slope of the outer retina PO_2 profile correlated with maximum outer retinal PO_2 ($R = 0.84$; $P < 0.0001$). Mean inner retina PO_2 correlated with maximum outer retinal PO_2 ($R = 0.88$; $P < 0.0001$).

Conclusions. A technique has been developed for quantitative mapping of retinal tissue oxygen tension with the potential to enable sequential monitoring of retinal oxygenation in health and disease. (*Invest Ophthalmol Vis Sci.* 2010;51:4766–4770) DOI:10.1167/iovs.09-4710

Retinal cells demand oxygen and nutrients to maintain normal metabolic function. Abnormalities in retinal oxygenation occur in acute retinal artery embolic disease, retinal vein occlusion, retinopathy of prematurity, and diabetic retinopathy[1–8] and are implicated in the development of glaucoma and age-related macular degeneration.[9,10] Development of technologies for assessment of retinal oxygenation can advance health care by providing a better understanding of disease pathophysiology and improving treatment outcomes.

Several techniques have been developed for assessment of oxygen delivery to the retinal tissue via choroidal and retinal circulations. Multiwavelength reflectance spectrophotometry measures oxygen saturation of blood,[11–15] phosphorescence lifetime imaging measures intravascular oxygen tension (PO_2),[16–21] and a laser Doppler method measures blood flow.[22–24] However, these techniques provide measurements only in the retinal vasculature and therefore are limited for assessment of retinal tissue PO_2.

Retinal tissue oxygenation has been evaluated by imaging methods and oxygen-sensitive microelectrodes. Magnetic resonance imaging[25–27] provides an indirect measure of retinal tissue PO_2, with limited resolution compared with optical techniques. A fluorescence imaging technique[28] has been reported for measurement of retinal tissue PO_2, but it has limited depth discrimination. Oxygen-sensitive microelectrodes[29–35] measure retinal tissue PO_2 directly with high-depth resolution. This technique is considered the gold standard, but it is invasive, requiring physical penetration of the tissue.

We have reported an optical imaging system for mapping of PO_2 in the retinal vasculature.[36–39] In the present study, we report a novel imaging technique for quantitative mapping of PO_2 at different depths of retinal tissue of rats. Lateral (along the retinal plane) and axial (through the retinal depth) variations in retinal tissue PO_2 were determined in three different fractions of inspired oxygen (FiO_2).

Materials and Methods

Animals

Thirteen male Long-Evans pigmented rats (450–650 g) were used. The animals were treated in compliance with the ARVO Statement for the Use of Animals in Ophthalmic and Vision Research. The rats were anesthetized using ketamine (85 mg/kg IP) and xylazine (3.5 mg/kg IP). An oxygen-sensitive molecular probe[40,41] (Oxyphor R2; Oxygen Enterprises, Ltd., Philadelphia, PA) was dissolved in saline and 3 μL (0.5 mM) was injected intravitreally. The presence of the probe in the vitreous was confirmed immediately after injection, by imaging the vitreous cavity with a slit lamp biomicroscope to visualize the bolus. The animals were imaged 24 hours after injection, an experimentally determined duration for the probe to diffuse from the vitreous into the retina. For monitoring systemic arterial PO_2, a catheter was placed in the femoral artery to obtain blood samples. Blood pressure and heart rate were monitored with a pressure transducer attached to the catheter and linked to a data-acquisition system (Biopac Systems Inc., Goleta, CA). Before imaging, the pupils were dilated with 2.5% phenylephrine and 1% tropicamide. Hydroxypropyl methylcellulose (1%) was applied to the cornea, and a glass coverslip was placed on the cornea to eliminate its refractive power and to prevent corneal dehydration. Normal body temperature was maintained with an animal holder connected to a water heater composed of copper tubing. FiO_2 was varied via a high-flow face mask system. Gas mixtures containing 10%, 21% (room air), and 50% oxygen were administered to the rats 10 minutes before and during imaging. Concurrent with imaging, arterial blood was drawn through the catheter without exposure to air, and systemic arterial PO_2 was measured with a blood gas analyzer (Radiometer, Westlake, OH). The rat was placed in front of the imaging instrument. The laser power was adjusted to 100 μW at the cornea. Because of pupil size, 40 μW entered the eye, yielding a retinal irradiance of approximately 30 mW/cm^2, which is safe for continuous viewing for 3600 seconds, according to the American National Standard Institute for Safety Standards.[42] Three images were acquired at

From the Department of Ophthalmology and Visual Sciences, University of Illinois at Chicago, Chicago, Illinois.

Supported by the National Eye Institute Grants EY17918 (MS) and EY01792 (UIC); a Research to Prevent Blindness (RPB), New York, NY, senior scientific investigator award (MS); and an unrestricted departmental award from RPB.

Submitted for publication September 29, 2009; revised October 8, 2009, and January 29 and February 23, 2010; accepted March 19, 2010.

Disclosure: **M. Shahidi**, None; **J. Wanek**, None; **N.P. Blair**, None; **D.M. Little**, None; **T. Wu**, None

Corresponding author: Mahnaz Shahidi, Department of Ophthalmology and Visual Sciences, University of Illinois at Chicago, 1855 West Taylor Street, Chicago IL 60612; mahnshah@uic.edu.

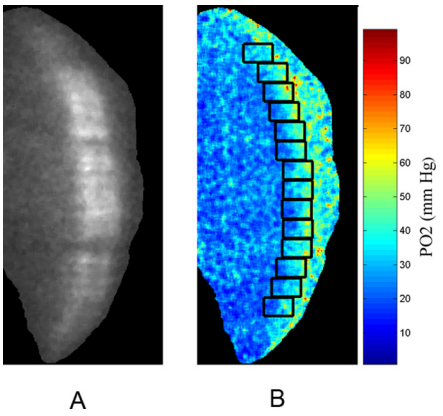

FIGURE 1. **(A)** An example of a phosphorescence image showing an optical section view through the depth of the retina. **(B)** Retinal PO_2 map generated from phase-delayed phosphorescence images. Color bar represents retinal PO_2 in mm Hg. Oxygen profiles were generated along the image at locations denoted by *rectangles*. The horizontal position of each rectangle was established based on the location of the maximum PO_2 in the posterior (*right*) portion of the retina, corresponding to 100% retinal depth.

each location within 2 disc diameters of the optic nerve head, over a period of approximately 60 seconds. Of the 13 rats, 3 were imaged in all three FiO_2 conditions, 5 in two, and 5 in one. In total, in each of the three FiO_2 conditions, data from eight rats were available, yielding a total of 24 data points.

Methods

The instrument for optical section phosphorescence imaging has been described.[36] Briefly, a narrow, focused, laser line was projected vertically at an angle on the retina, and the phosphorescence of the oxygen-sensitive molecular probe was imaged. Because of the 10° angle between the incident laser and imaging path, an optical section phosphorescence image was acquired by a digital camera. Phosphorescence was imaged by matching the laser wavelength (532 nm) to the excitation wavelength of the molecular probe and placing a filter with transmission overlapping the phosphorescence emission in the imaging path. The phosphorescence lifetime was measured with a frequency-domain approach, as published elsewhere.[20,36,43,44] According to the principles of this approach, the laser light and sensitivity of the camera were independently modulated at a frequency of 1600 Hz. The phase between the two modulators was incrementally delayed at 74-μs intervals and a set of 10 optical section phosphorescence images were acquired. The phase-delayed images were analyzed to determine phosphorescence lifetime, which is related to PO_2 according to the Stern-Volmer expression: $\tau_0/\tau = 1 + (\kappa_Q)(\tau_0)(PO_2)$, where PO_2 (mm Hg) is the oxygen tension, τ (in microseconds) is the phosphorescence lifetime, κ_Q (1/mm Hg μs) is the quenching constant for the triplet-state phosphorescence probe, and τ_0 is the lifetime in a zero-oxygen environment.[40] A small error in retinal PO_2 calculations may be present, since the constants of the Stern-Volmer relation are not known precisely in tissue. A retinal PO_2 map was generated by calculating PO_2 at each pixel on the image and three repeated PO_2 maps were obtained at the same location per eye. In phosphorescence intensity images, a boundary between the retina and vitreous was visible. The location of the boundary on the phosphorescence image coincided with the vitreoretinal interface that was clearly visualized on the reflectance image. The retinal region was isolated by generating a mask by global thresholding of the phosphorescence intensity image with an iterative threshold-selection method.[45] The mask assigned a value of 0 to PO_2 map pixels with corresponding intensity values below a threshold on the phosphorescence intensity image.

The masked retinal PO_2 map was sectioned by contiguous rectangular segments along the image from superior to inferior. Each segment was 20 pixels (100 μm) vertically and spanned the retinal depth. The horizontal position of each segment was established on the basis of the location of the maximum PO_2 level in the posterior portion of the retina, corresponding to 100% retinal depth. The number of segments in each PO_2 map varied, depending on the vertical extent of the retina that could be visualized. Retinal PO_2 maps were sectioned into 13 ± 1 segments (mean ± SD; n = 24). In each segment, a PO_2 profile was obtained by vertically integrating pixel values over the segment (20 pixels). The resulting profile displayed PO_2 values at 30 retinal depth locations. A total of 13 oxygen profiles were generated from 13 contiguous segments along each retinal PO_2 map. The outer and inner retinal areas in an oxygen profile were defined by the region spanning 50% to 100% and <50% of the retinal depth, respectively. An average and SD for the following measures were calculated from oxygen profiles: maximum and minimum outer retina PO_2, mean inner retina PO_2, and slope of the outer retina PO_2 profile between 75% and 100% of the retinal depth.

The reliability of measurements was established in two separate complementary analyses. First, intraclass correlations were calculated between repeated images in each eye on PO_2 profiles. Second, the effect of location and repeatability on PO_2 measurements was examined by subjecting the data to a two-way analysis of variance (ANOVA), with location and image as between-samples repeated measures. A significant main effect of image suggests differences between the repeated images that would make it difficult to apply the technique reliably. The main effect of location indicates variations at different locations along the image. Interactions between the two (image, location) indicate that measurement variability changes in a systematic manner between repeated images as a function of location. ANOVA was used to compare measurements obtained during 10%, 21%, and 50% FiO_2. Linear regression analysis was performed to relate systemic arterial PO_2, slope of the outer retina PO_2 profile, and mean inner retina PO_2 to maximum outer retina PO_2. Statistical significance was accepted at $P < 0.05$.

Results

Blood pressure was 90 ± 15 (mean ± SD), 139 ± 25, and 135 ± 21 mm Hg (significant change at P = 0.0002); heart rate was 257 ± 17, 278 ± 46, and 241 ± 23 beats per minute (P = 0.08); and systemic arterial PO_2 measurements were 39 ± 11,

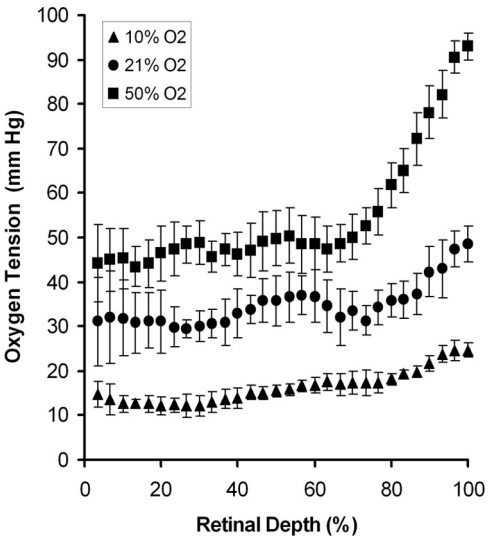

FIGURE 2. Oxygen profiles derived from retinal PO_2 maps generated with 10%, 21%, and 50% FiO_2 are shown. Each profile was obtained from a single segment of a retinal PO_2 map. Error bars represent standard deviations.

TABLE 1. Effects of Image (Repeated-Measurement Variability) and Location (Lateral Variations) on Retinal PO_2 with 10%, 21%, and 50% FiO_2

	Maximum Outer Retina PO_2		Minimum Outer Retina PO_2		Mean Inner Retina PO_2	
FiO_2 Effect	***F***	***P***	***F***	***P***	***F***	***P***
10%						
Image	0.640	0.542	0.298	0.747	0.817	0.614
Location	0.374	0.954	1.067	0.399	0.023	0.978
Image/location	0.746	0.746	0.433	0.984	1.095	0.361
21%						
Image	0.153	0.860	0.141	0.870	0.227	0.800
Location	0.971	0.478	0.892	0.546	0.907	0.533
Image/location	0.730	0.789	0.729	0.789	0.740	0.778
50%						
Image	0.917	0.422	0.713	0.507	1.110	0.357
Location	0.736	0.689	0.801	0.628	0.665	0.753
Image/location	1.052	0.407	0.748	0.770	1.167	0.292

54 ± 7, and 156 ± 40 mm Hg (significantly different at $P < 0.0001$) with 10%, 21%, and 50% FiO_2, respectively.

An example of an optical section phosphorescence image, displaying a cross-sectional view of the retina in a rat during 21% FiO_2 is shown in Figure 1A. The phosphorescence from the oxygen probe is visualized distinctly in the retinal tissue. A retinal PO_2 map was generated from the phase-delayed optical section phosphorescence images, as shown in Fig. 1B. The locations of contiguous segments along the image are marked by rectangles. Retinal PO_2 was highest at the choroidal interface and decreased incrementally through the outer retinal depth. Examples of oxygen profiles derived from retinal PO_2 maps generated in 10%, 21%, and 50% FiO_2 are shown in Figure 2. Each profile was obtained from a single segment of a retinal PO_2 map. Systemic arterial PO_2 was 28, 50, and 109 mm Hg for the three profiles derived with 10%, 21%, and 50% FiO_2, respectively. In the outer retina, PO_2 decreased linearly from a maximum PO_2 level in the proximity of the choroid and reached a minimum PO_2 at the location corresponding to the photoreceptor cell inner segment, as previously reported.[34] In the inner retina, PO_2 was relatively constant but displayed spatial variations because of the retinal vascular architecture.[34]

All measures of maximum and minimum outer retina PO_2, and mean inner retina PO_2 were consistent. Intraclass correlations were greater than 0.94, 0.75, and 0.44 in 10%, 21%, and 50% FiO_2 conditions, respectively ($P < 0.001$). The results of two-way ANOVA analysis for determining the effects of image and location on PO_2 measurements are shown in Table 1. There were no significant effects of image, location, or interaction between the two effects on maximum or minimum outer retina PO_2 or mean inner retina PO_2 with 10%, 21%, or 50% FiO_2 ($P \geq 0.3$).

Maximum outer retina PO_2 measurements obtained with 10%, 21%, and 50% FiO_2 were 37 ± 15, 57 ± 20, and 94 ± 23 mm Hg, respectively, and increased significantly with higher FiO_2 ($P < 0.0001$). Maximum outer retina PO_2 correlated with systemic arterial PO_2 ($R = 0.70$; $P < 0.0001$; $n = 24$). Maximum and minimum outer retina PO_2 and mean inner retina PO_2 measurements obtained in 10%, 21%, and 50% FiO_2 are shown in Figure 3. Mean inner retina and minimum outer retina PO_2 measurements were significantly different during the three oxygen breathing conditions ($P = 0.001$ and $P = 0.0003$, respectively).

The relationship between the slope of outer retina oxygen profile and maximum outer retina PO_2 is shown in Figure 4. The slope of the outer retina PO_2 profile was correlated with maximum outer retina PO_2 ($R = -0.86$; $P < 0.0001$; $n = 24$). The relationship between mean inner retina PO_2 and maximum outer retina PO_2 is shown in Figure 5. Mean inner retina PO_2 correlated highly with maximum outer retina PO_2 ($R = 0.88$; $P < 0.0001$; $n = 24$).

DISCUSSION

Development of retinal pathologies may be related to retinal tissue hypoxia in common retinal diseases, such as diabetic retinopathy and age-related macular degeneration. Therefore, technologies that provide direct measurement of retinal tissue PO_2 are needed to provide better understanding of the role of

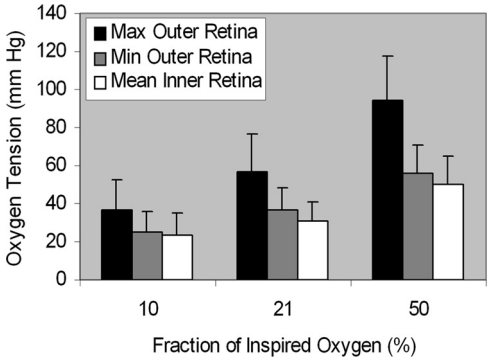

FIGURE 3. Mean retinal PO_2 measurements obtained with 10%, 21%, and 50% FiO_2 in eight rats. Error bars, SD.

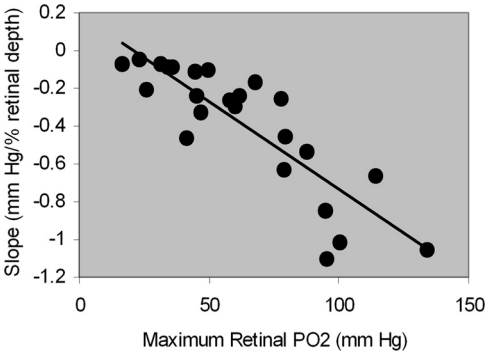

FIGURE 4. The relationship between the slope of the outer retina PO_2 profile and maximum outer retina PO_2. The more negative values correspond to a steeper slope.

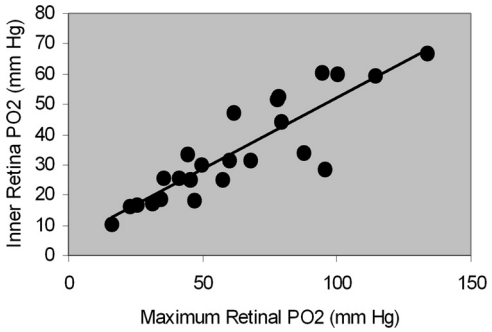

FIGURE 5. The relationship between mean inner retina PO_2 and maximum outer retina PO_2.

hypoxia in these retinal diseases. In the present study, an imaging technique was reported for mapping of retinal tissue PO_2 and generating PO_2 profiles through the retinal depth. The feasibility of the technique was established by determining reproducibility of PO_2 measurements and demonstrating a significant increase in inner and outer retinal PO_2 with higher fractions of inspired oxygen.

Significant changes in systemic arterial PO_2 were induced by varying the fraction of inspired oxygen. In 21% and 50% FiO_2, systemic arterial PO_2 was lower than measurements obtained in previous studies.[46–48] This result is attributable to the hypoxic condition of the rats in our study caused by the respiratory depressant effect of the anesthetics.[37] Maximum outer retina PO_2 significantly increased according to higher fractions of inspired oxygen, in agreement with prior studies that showed a proportionate increase in choroidal PO_2 under hyperoxia.[49] As previously reported, maximum outer retina and systemic arterial PO_2 measurements were similar under hypoxia.[32,39] In the 50% FiO_2, maximum outer retina PO_2 was approximately 50% of systemic arterial PO_2, in agreement with studies performed under systemic arterial $PO_2 > 80$ mm Hg in rats and other species.[32,46,50,51] Mean inner and minimum outer retina PO_2 increased with higher fractions of inspired oxygen, corresponding to microelectrode data in the cat and the rat.[30,46,49] Similar to previous studies using oxygen microelectrodes that found larger outer retina PO_2 gradients with increased FiO_2,[52] steeper slopes of the outer retina PO_2 profile were linearly correlated with higher maximum outer retina PO_2, indicating that oxygen flux into the outer retina is increased when maximum outer retina PO_2 is higher.

Oxygen profiles generated by the optical imaging technique in the present study displayed different features compared with those published using the microelectrode technique.[34,46] Inner retina PO_2 variations did not display a minimum between two capillary layers, and the gradient of outer retina PO_2 was lower. Since the imaging technique uses phosphorescent light for measuring retinal PO_2, scattered light from intraretinal structures may have reduced the signal-to-noise ratio of the system, thereby limiting detection of PO_2 variations due to inner retina capillary beds. In addition, the contribution of scattered light may have caused the averaging of phosphorescence signals from different retinal depths. This averaging would effectively lower the maximum outer retina PO_2 measurement and elevate the minimum outer retina PO_2 measurement, resulting in a reduced outer retina oxygen gradient compared with microelectrode data.

Although the retinal irradiance used in the present study was below the level that produces tissue damage, repeated laser exposures have the potential to induce phototoxic injury.[53] Phototoxicity would have resulted in a progressive effect on data derived from images acquired repeatedly at the same location. However, data obtained from consecutive images acquired at the same location were found to be highly reproducible. Furthermore, the functional and structural integrity of the retinal tissue was assessed with available techniques after imaging in selected rats. In a light-adapted condition, the maximum amplitudes of the b-wave of the electroretinograms recorded 24 hours after probe and saline intravitreal injections were found to be similar, and retinal structures imaged by optical coherence tomography after PO_2 imaging displayed no abnormalities. Future studies are needed to thoroughly assess the potential presence of phototoxicity in the retinal tissue and establish the reliability of the technique for monitoring disease progression over time.

Retinal PO_2 measurements were reproducible, providing a reliable means of assessment of retinal oxygenation and metabolism due to retinal diseases. Furthermore, variations in maximum and minimum outer and mean inner retina PO_2 at different locations along the image were small; suggesting that retinal PO_2 profiles were relatively constant in the spatial extent imaged. One potential limitation of this technique is the dependence of the data on the quality of acquired images, which is a factor in all optical imaging techniques. Blurring of images can occur due to media opacities and aberrations, affecting accuracy of PO_2 measurements. In our data set, this type of image degradation was encountered in approximately 20% of animals, in which the maximum outer retina PO_2 was significantly lower than the systemic arterial PO_2. In the present study, only focused images were analyzed, to minimize inaccuracy due to image blurring. Overall, this technique for quantitative mapping of retinal PO_2 in animals may become useful for sequential monitoring of retinal oxygenation and provide a reliable means for assessing treatment regimens for retinal diseases.

References

1. Yoneya S, Saito T, Nishiyama Y, et al. Retinal oxygen saturation levels in patients with central retinal vein occlusion. *Ophthalmology.* 2002;109:1521–1526.
2. Dugan JD Jr, Green WR, Shonat RD, Kight AC. Ophthalmologic manifestations of carotid occlusive disease. *Eye.* 1991;5:226–238.
3. Zhang W, Ito Y, Berlin E, Roberts R, Berkowitz BA. Role of hypoxia during normal retinal vessel development and in experimental retinopathy of prematurity. *Invest Ophthalmol Vis Sci.* 2003;44:3119–3123.
4. Stefansson E, Machemer R, de Juan E Jr, McCuen BW II, Peterson J. Retinal oxygenation and laser treatment in patients with diabetic retinopathy. *Am J Ophthalmol.* 1992;113:36–38.
5. Linsenmeier RA, Braun RD, McRipley MA, et al. Retinal hypoxia in long-term diabetic cats. *Invest Ophthalmol Vis Sci.* 1998;39:1647–1657.
6. Berkowitz BA, Kowluru RA, Frank RN, Kern TS, Hohman TC, Prakash M. Subnormal retinal oxygenation response precedes diabetic-like retinopathy. *Invest Ophthalmol Vis Sci.* 1999;40:2100–2105.
7. Berkowitz BA, Luan H, Gupta RR, et al. Regulation of the early subnormal retinal oxygenation response in experimental diabetes by inducible nitric oxide synthase. *Diabetes.* 2004;53:173–178.
8. Bursell SE, Clermont AC, Shiba T, King GL. Evaluating retinal circulation using video fluorescein angiography in control and diabetic rats. *Curr Eye Res.* 1992;11:287–295.
9. Anderson DR. Is ischemia the villain in glaucomatous cupping and atrophy? In: Brockhurst RJ, Boruchoff SA, Hutchinson BT, Lessell S, eds. *Controversy in Ophthalmology*. Philadelphia: W.B. Saunders Co.; 1977:312–319.
10. Zarbin MA. Age-related macular degeneration: review of pathogenesis. *Eur J Ophthalmol.* 1998;8:199–206.
11. Delori FC. Noninvasive technique for oximetry of blood in retinal vessels. *Appl Opt.* 1988;27:1113–1125.
12. Smith MH, Denninghoff KR, Hillman LW, Chipman RA. Oxygen saturation measurements of blood in retinal vessels during blood loss. *J Biomed Opt.* 1998;3:296–303.

13. Schweitzer D, Thamm E, Hammer M, Kraft J. A new method for the measurement of oxygen saturation at the human ocular fundus. *Int Ophthalmol.* 2001;23:347–353.
14. Hammer M, Schweitzer D. Quantitative reflection spectroscopy at the human ocular fundus. *Phys Med Biol.* 2002;47:179–191.
15. Denninghoff KR, Smith MH, Lompado A, Hillman LW. Retinal venous oxygen saturation and cardiac output during controlled hemorrhage and resuscitation. *J Appl Physiol.* 2003;94:891–896.
16. Wilson DF, Vanderkooi JM, Green TJ, Maniara G, DeFeo SP, Bloomgarden DC. A versatile and sensitive method for measuring oxygen. *Adv Exp Med Biol.* 1987;215:71–77.
17. Rumsey WL, Vanderkooi JM, Wilson DF. Imaging of phosphorescence: a novel method for measuring oxygen distribution in perfused tissue. *Science.* 1988;241:1649–1651.
18. Shonat RD, Wilson DF, Riva CE, Pawlowski M. Oxygen distribution in the retinal and choroidal vessels of the cat as measured by a new phosphorescence imaging method. *Appl Optics.* 1992;31:3711–3718.
19. Riva CE. Noninvasive measurement of oxygen tension in the optic nerve head. *Curr Opin Ophthalmol.* 1998;9:56–60.
20. Shonat RD, Kight AC. Oxygen tension imaging in the mouse retina. *Ann Biomed Eng.* 2003;31:1084–1096.
21. Ferrez PW, Chamot SR, Petrig BL, Pournaras CJ, Riva CR. Effect of visual stimulation on blood oxygenation in the optic nerve head of miniature pigs: a pilot study. *Klin Monatsbl Augenheilkd.* 2004;221:364–366.
22. Petrig BL, Riva CE, Hayreh SS. Laser Doppler flowmetry and optic nerve head blood flow. *Am J Ophthalmol.* 1999;127:413–425.
23. Longo A, Geiser M, Riva CE. Subfoveal choroidal blood flow in response to light-dark exposure. *Invest Ophthalmol Vis Sci.* 2000;41:2678–2683.
24. Falsini B, Riva CE, Logean E. Flicker-evoked changes in human optic nerve blood flow: relationship with retinal neural activity. *Invest Ophthalmol Vis Sci.* 2002;43:2309–2316.
25. Berkowitz RA, Klyce SD, Kaufman HE. Aqueous hyposecretion after penetrating keratoplasty. *Ophthalmic Surg.* 1984;15:323–324.
26. Ito Y, Berkowitz BA. MR studies of retinal oxygenation. *Vision Res.* 2001;41:1307–1311.
27. Roberts R, Zhang W, Ito Y, Berkowitz BA. Spatial pattern and temporal evolution of retinal oxygenation response in oxygen-induced retinopathy. *Invest Ophthalmol Vis Sci.* 2003;44:5315–5320.
28. Zuckerman R, Cheasty JE, Wang Y. Optical mapping of inner retinal tissue PO2. *Curr Eye Res.* 1993;12:809–825.
29. Linsenmeier RA. Effects of light and darkness on oxygen distribution and consumption in the cat retina. *J Gen Physiol.* 1986;88:521–542.
30. Linsenmeier RA, Yancey CM. Effects of hyperoxia on the oxygen distribution in the intact cat retina. *Invest Ophthalmol Vis Sci.* 1989;30:612–618.
31. Alder VA, Cringle SJ. Vitreal and retinal oxygenation. *Graefes Arch Clin Exp Ophthalmol.* 1990;228:151–157.
32. Linsenmeier RA, Braun RD. Oxygen distribution and consumption in the cat retina during normoxia and hypoxemia. *J Gen Physiol.* 1992;99:177–197.
33. Linsenmeier RA, Padnick-Silver L. Metabolic dependence of photoreceptors on the choroid in the normal and detached retina. *Invest Ophthalmol Vis Sci.* 2000;41:3117–3123.
34. Cringle SJ, Yu DY, Yu PK, Su EN. Intraretinal oxygen consumption in the rat in vivo. *Invest Ophthalmol Vis Sci.* 2002;43:1922–1927.
35. Wangsa-Wirawan ND, Linsenmeier RA. Retinal oxygen: fundamental and clinical aspects. *Arch Ophthalmol.* 2003;121:547–557.
36. Shahidi M, Shakoor A, Shonat R, Mori M, Blair NP. A method for measurement of chorioretinal oxygen tension. *Curr Eye Res.* 2006;31:357–366.
37. Shakoor A, Gupta M, Blair NP, Mori M, Shahidi M. Chorioretinal vascular oxygen tension in spontaneously breathing anesthetized rats. *Ophthalmic Res.* 2007;39:103–107.
38. Shakoor A, Blair NP, Mori M, Shahidi M. Chorioretinal vascular oxygen tension changes in response to light flicker. *Invest Ophthalmol Vis Sci.* 2006;47:4962–4965.
39. Shahidi M, Wanek J, Blair NP, Mori M. Three-dimensional mapping of chorioretinal vascular oxygen tension in the rat. *Invest Ophthalmol Vis Sci.* 2009;50:820–825.
40. Dunphy I, Vinogradov SA, Wilson DF. Oxyphor R2 and G2: phosphors for measuring oxygen by oxygen-dependent quenching of phosphorescence. *Anal Biochem.* 2002;310:191–198.
41. Vinogradov SA, Lo L-W, Wilson DF. Dendritic polyglutamic porphyrins: Probing porphyrin protection by oxygen-dependent quenching of phosphorescence. *Chem Eur J.* 1999;5:1338–1347.
42. ANSI. American National Standard for Safe Use of Lasers. ANSI Z136.1-1993. Orlando, FL: The Laser Institute of America; 1993.
43. Lakowicz JR, Laczko G, Cherek H, Gratton E, Limkeman M. Analysis of fluorescence decay kinetics from variable-frequency phase shift and modulation data. *Biophys J.* 1984;46:463–477.
44. Lakowicz JR, Szmacinski H, Nowaczyk K, Berndt KW, Johnson M. Fluorescence lifetime imaging. *Anal Biochem.* 1992;202:316–330.
45. Ridler TW, Calvard S. Picture thresholding using an iterative selection method. *IEEE Trans Syst Man Cybernet.* 1978;SMC-8:630–632.
46. Yu DY, Cringle SJ. Oxygen distribution and consumption within the retina in vascularised and avascular retinas and in animal models of retinal disease. *Prog Retin Eye Res.* 2001;20:175–208.
47. Torbati D, Totapally BR, Camacho MT, Wolfsdorf J. Experimental critical care in ventilated rats: effect of hypercapnia on arterial oxygen-carrying capacity. *J Crit Care.* 1999;14:191–197.
48. Sumitra M, Manikandan P, Rao KV, Nayeem M, Manohar BM, Puvanakrishnan R. Cardiorespiratory effects of diazepam-ketamine, xylazine-ketamine and thiopentone anesthesia in male Wistar rats: a comparative analysis. *Life Sci.* 2004;75:1887–1896.
49. Yu DY, Cringle SJ, Alder V, Su EN. Intraretinal oxygen distribution in the rat with graded systemic hyperoxia and hypercapnia. *Invest Ophthalmol Vis Sci.* 1999;40:2082–2087.
50. Yu DY, Cringle SJ, Su EN. Intraretinal oxygen distribution in the monkey retina and the response to systemic hyperoxia. *Invest Ophthalmol Vis Sci.* 2005;46:4728–4733.
51. Pournaras CJ, Riva CE, Tsacopoulos M, Strommer K. Diffusion of O2 in the retina of anesthetized miniature pigs in normoxia and hyperoxia.1989;49:347–360.
52. Cringle SJ, Yu DY. A multi-layer model of retinal oxygen supply and consumption helps explain the muted rise in inner retinal PO(2) during systemic hyperoxia. *Comp Biochem Physiol A Mol Integr Physiol.* 2002;132:61–66.
53. Stepinac TK, Chamot SR, Rungger-Brandle E, et al. Light-induced retinal vascular damage by Pd-porphyrin luminescent oxygen probes. *Invest Ophthalmol Vis Sci.* 2005;46:956–966.